EXPECTED SCIENTIFIC RESULTS ON BALLISTIC SPACECRAFT MISSIONS TO COMET ENCKE DURING THE 1980 APPARITION*

Michael J. Mumma

INTRODUCTION

This paper summarizes three proposed ballistic spacecraft missions to intercept P/Encke during the 1980 apparition, establishes a baseline physical activity model for P/Encke, and assesses the performance of the neutral mass spectrometer and of the imaging experiment on each intercept mission.[1]

Many of the most fundamental questions about comets are unlikely ever to be answered by ground-based or near-earth observations alone, and a direct intercept of a comet by an appropriately instrumented spacecraft is required in order to directly study the comet and its interaction with the solar wind.[2-5]

There is general agreement on the most obvious scientific goals of such a mission but, until now, a quantitative estimate of the possibilities of achieving these goals had not been made. Because of the long lead times required by deep space missions, the next good opportunity for intercepting a short-period comet occurs in 1980, for Encke's comet. Encke's comet has been studied from the ground for more than 150 years and from space recently, and sufficient data now are available to enable making reasonably accurate estimates of the expected scientific value of a direct intercept of this comet.

The problem of assessing the relative scientific merit of various ballistic flyby missions to Comet Encke requires: (1) a determination of the physical activity model for the comet, (2) a careful study of the ephemeris errors[6] and a determination of the consequent miss-distances for various missions, (3) a determination of the flyby velocities, and (4) knowledge of the sensitivities of particular instruments which could be carried on the cometary spacecraft. Each point will be addressed

ORIGINAL PAGE IS OF POOR QUALITY

---

in this paper and the results will be used to establish physically
realistic estimates of the expected scientific results of the various
missions.

The scientific goals have been discussed at length by various
earlier groups and can be divided into the following areas: (1) studies
of the nucleus, (2) studies of dust and of the neutral and ionized gaseous
components, and (3) study of the solar wind interaction with the comet
through in-situ measurements of the electromagnetic fields and the
particles. Two experiments are found to be particularly sensitive to
the mission mode, i.e. the experiment for taking images of the nucleus,
and the neutral mass spectrometer experiment for measurement of parent
molecules in the inner coma. The quality of the data obtained with these
two experiments depends principally on three factors: (1) the heliocentric
distance at the time of intercept (determines the comet's activity and the
crossing-angle of the spacecraft trajectory with the sun-comet line), (2)
the spacecraft velocity relative to the comet (determines the time dura-
tion of the encounter), and (3) the targeting accuracy and minimum distance
of approach to the nucleus (determines the amount of time spent within the
icy halo and in regions of relatively high gas densities).

MISSION PARAMETERS

The orbital characteristics of Comet Encke are shown in Fig. 1.[7]
The flyby velocity and crossing-angle are shown for various spacecraft
launch dates and heliocentric intercept distances in Fig. 2 and 3. The
three missions studied correspond to intercepts at 0.34 AU (Encke's
perihelion), at 0.53 AU, and at 0.8 AU. These heliocentric distances
were suggested by: (1) the cometary activity model (most active near peri-
helion), (2) the need for low flyby velocities (lowest near perihelion),

ORBITAL ELEMENTS (EQUINOX 1950.0)

EPOCH	1980 NOV. 17.0
T	1980 DEC. 6.57610
q	0.3399411 AU
e	0.8467578
Ω	334.19764°
ω	185.97967°
i	11.94599°

EPOCH	1984 APR. 10.0
T	1984 MAR. 27.68721
q	0.3410024 AU
e	0.8463305
Ω	334.18436°
ω	185.99329°
i	11.92738°

——————— ABOVE ECLIPTIC

— — — — — BELOW ECLIPTIC

⊕ EARTH AT ENCKE PERIHELIA

2 AU

LINE OF NODES

MAR. 27, 1984 ⊕

P

SUN

50

⊕ DEC 6, 1980

100
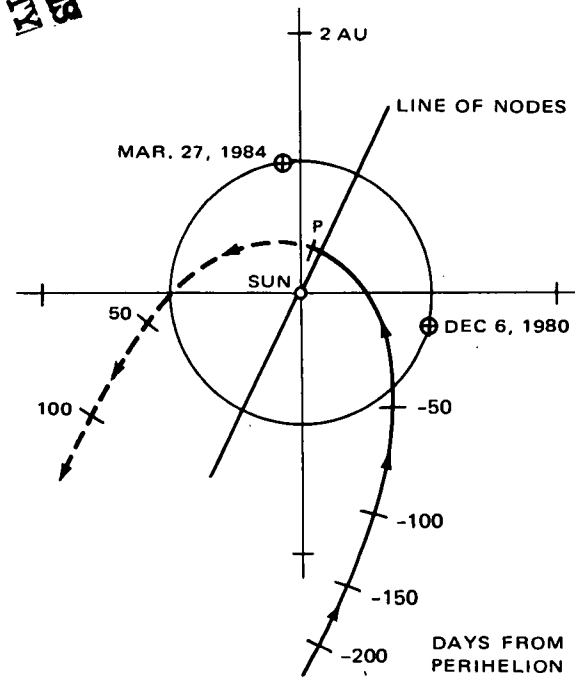
−50

−100

−150

−200

DAYS FROM
PERIHELION

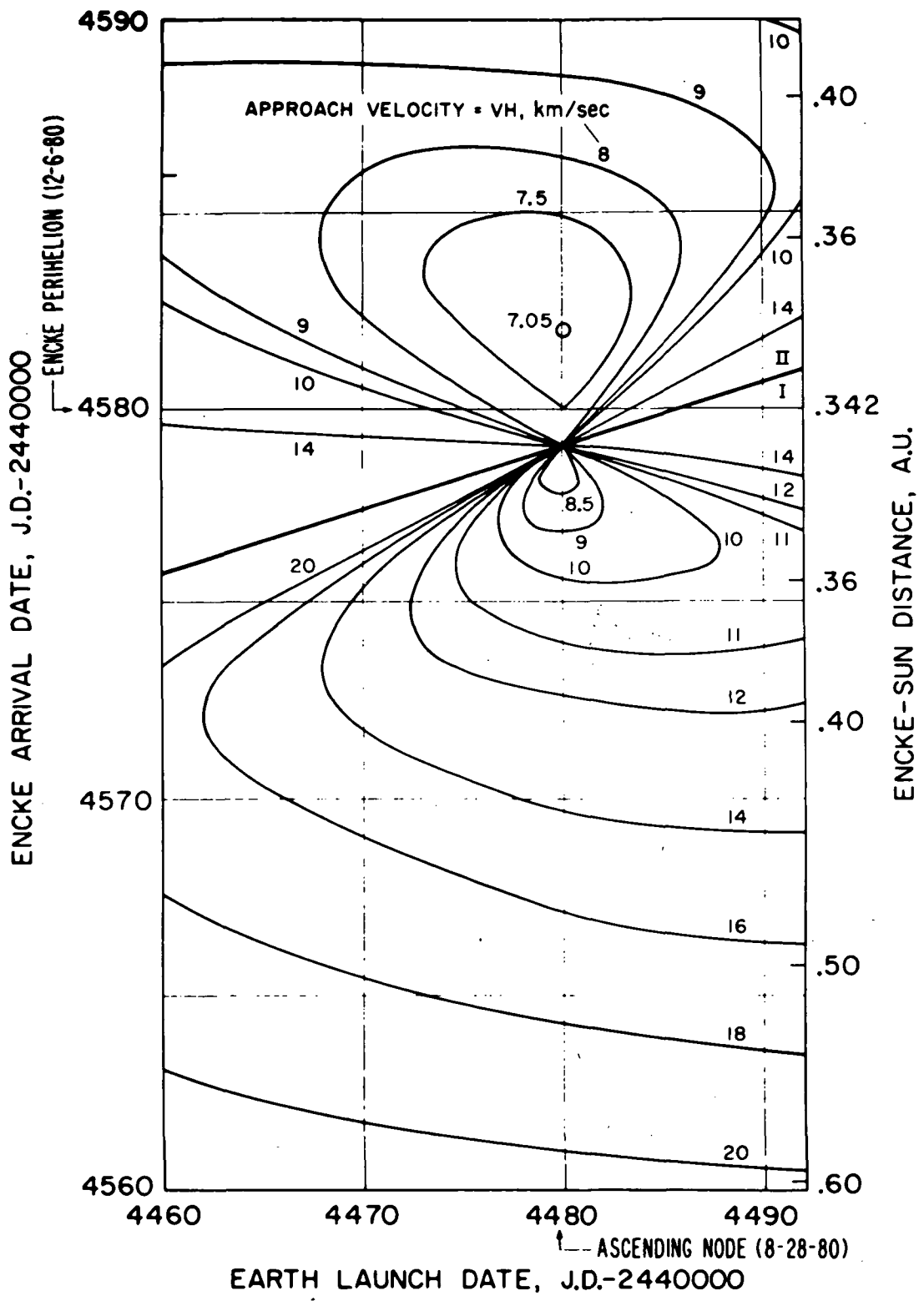FIG. 1 - Orbital Characteristics of P/Encke

FIG. 2 - Spacecraft Velocity Relative to
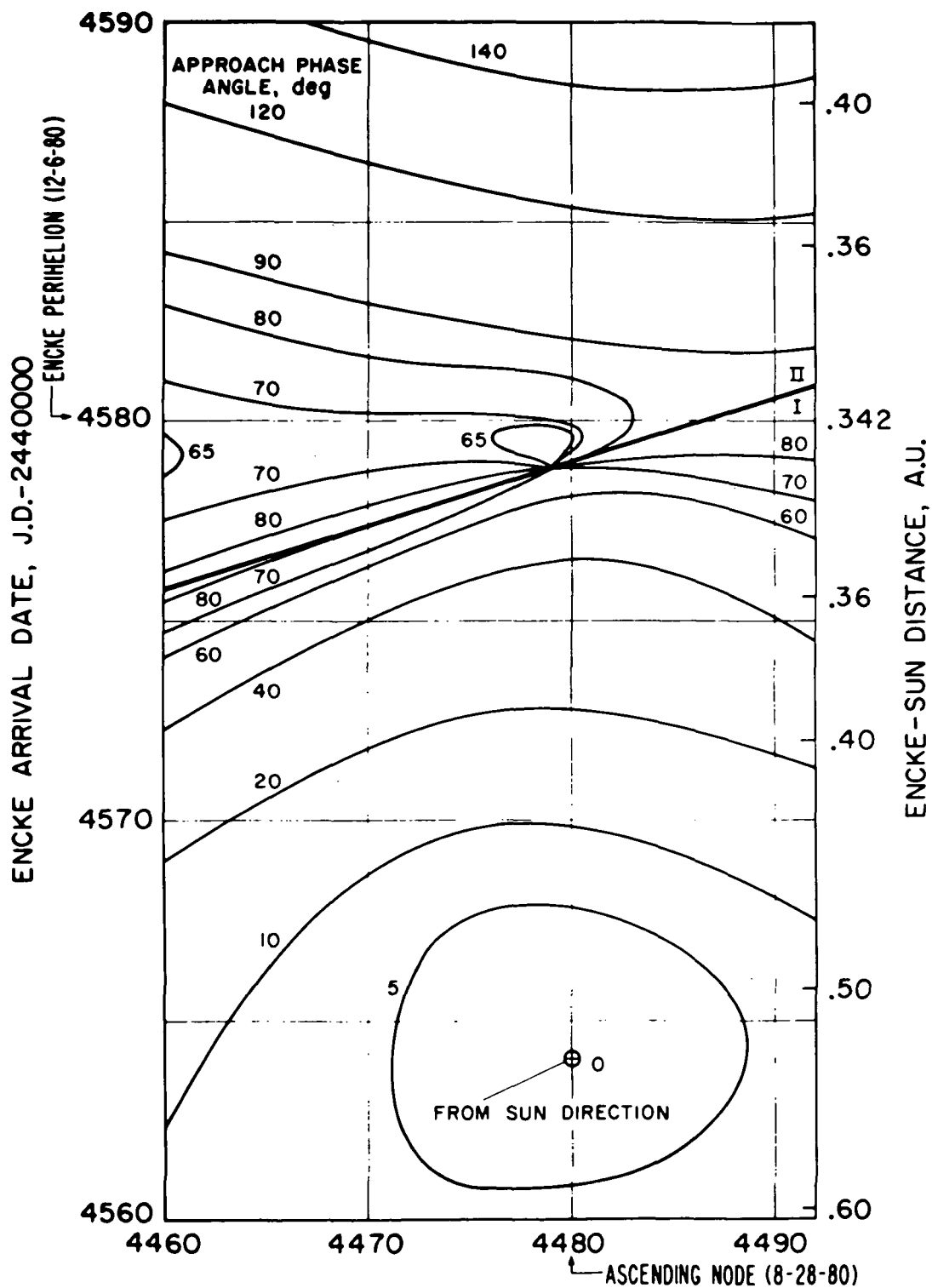P/Encke (Flyby Velocity)

FIG. 3 - Crossing-Angle vs. Launch Date and
R(AU) at Intercept

(3) the encounter geometry which determines the regions of the comet traversed by the spacecraft (the crossing-angle is zero at 0.53 AU), and (4) launch vehicle delivery characteristics and budgetary considertions (spacecraft orbits for cometary intercepts smaller than ~ 0.53 AU require the very expensive Titan-Centaur launch vehicle whereas intercepts at R $\gtrsim$ .53 AU can be achieved using the relatively less expensive Atlas-Centaur launch vehicle). The nominal values of specific mission parameters such as heliocentric distance at the time of intercept (R), earth-comet distance at intercept (Δ), relative flyby velocity, etc. are shown in Table I. The achievable miss distances (impact parameters, to the atomic physicists) will be discussed later.

The spacecraft trajectories with respect to the sun-comet line are shown in Fig. 4. The crossing-geometries at closest approach are quite different for the perihelion intercept (P+2), where the crossing-angle is in the range $70^{\circ} - 90^{\circ}$, and for the P-15 and P-30 intercepts where the crossing-angle is $< 20^{\circ}$. Also, the trajectory at P+2 has a curious 'fish-hook' shape which allows two bow-shock crossings and two traversals of the coma. However, a separate probe would be required for making measurements in the tail. The tail-probe could be launched on the same rocket with the coma-probe and would follow a trajectory similar to that of the coma probe but displaced tail-ward from the nucleus by as much as several tens of thousands of kilometers. The crossing of the tail at high angles suggests that filaments will be traversed in times short compared with temporal variations in the comet's activity so that spatial-temporal effects could be separated. The geometry at closest approach for such an intercept is shown in Fig. 5. The opportunity for simultaneous correlative measurements during cometary

1002

FIG. 4 ENCOUNTER GEOMETRY
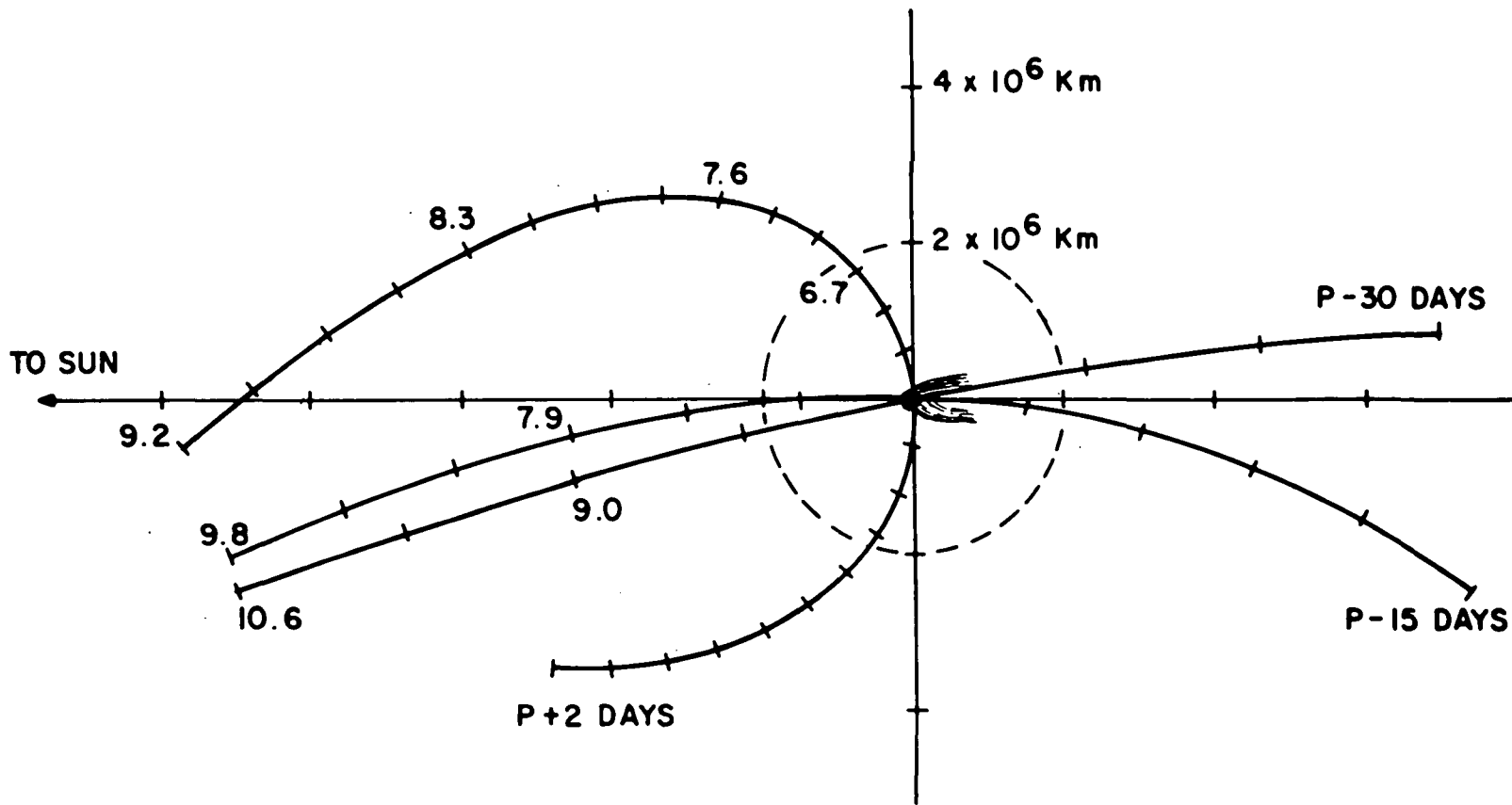
S/C TRAJECTORY TIC MARKS
AT ONE DAY INTERVALS
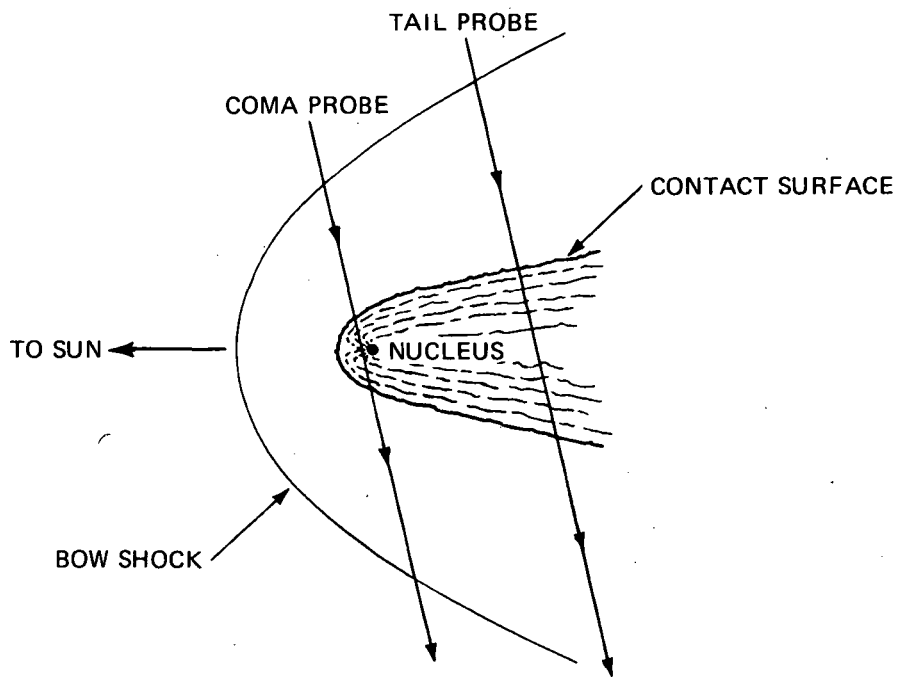
FIG. 5 - Crossing Geometry on the Perihelion
Intercept

NOMINAL MISSION PARAMETERS

MISSION:	1	2	3
R(AU)	.34	.53	.80
DATE	P+2 *	P-15	P-30
$\triangle$(AU)	1.1	.58	.34
$C_3(KM^2/S^2)$ **	94	72	43
FLYBY SPEED (KM/SEC)	8	18	26
THERMAL LOAD	8.7	3.6	1.6
MISS DISTANCE	VARIABLE		

* Two days after perihelion passage (P).

** Required launch injection energy.

encounter and also in the interplanetary cruise mode is obvious. On the other hand, during either the P-15 or P-30 intercept missions both coma and tail would be traversed by a single spacecraft. The thermal environment (insolation) is less severe at these greater heliocentric distances, but the comet's activity is reduced and the relative space-craft velocity is larger, affording less measurement time.

The targeting strategy is affected to some extent by the need to pass on the sunward side of the nucleus to ensure good quality images (Fig. 6). The spacecraft may be targeted on the nucleus (case B) for the P-15 and P-30 intercepts, but it should be targeted sunward of the nucleus in the P+2 mission (case C). If the estimated impact hazard from dust particles were to demonstrate the existence of an 'exclusion-zone' which the spacecraft should not enter, the targeting strategy would be as shown in case A.

Median miss distances were determined from the three-standard-deviation (3-σ) error ellipses by calculating the probability density lying between R and R + dR, i.e. P(R)dR in Fig. 6. The starting point was the set of a-priori ephemeris errors (Yeomans[6]) which are unusually small because the non-gravitational effects on Encke's motion (particularly A_2) are quite small (Fig. 7). The a-priori ephemeris errors for 1980 were improved by assuming ground-based observations prior to launch and before intercept. The (3-σ) targeting error ellipses were then calculated and the median miss distances were determined for various combinations of targeting strategies, and for the absence or presence of on-board navigation (Table II). The median miss distances (3-σ) were found to be ~100 Km with successful on-board navigation and ~ 500 Km without it, assuming no exclusion zone.

CASE I : TARGETING STRATEGY ASSUMING AN EXCLUSION
ZONE OF RADIUS R_{EZ}. $R_\oplus = 0.34; 0.53; 0.8$ AU

P(R) dR

3 σ TARGETING
ERROR ELLIPSE

N

EXCLUSION ZONE
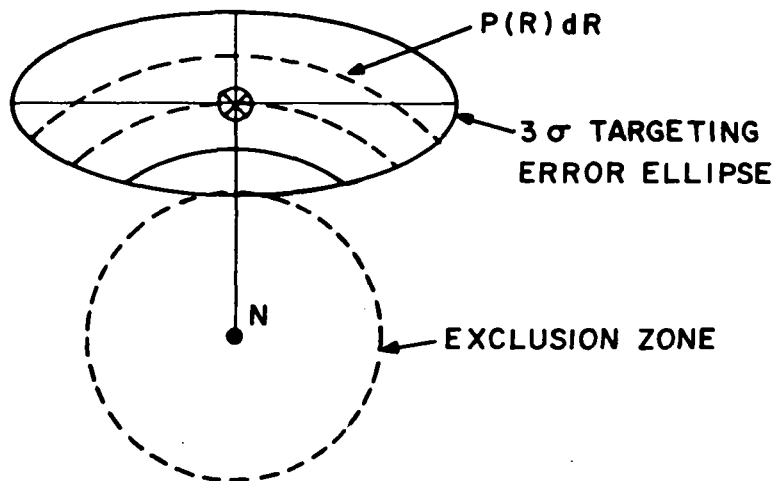
CASE 2 : TARGETING STRATEGY WHEN APPROACHING FROM
SUN ALONG THE SUN - COMET LINE. $R_{EZ} = 0$
$R_\oplus = 0.8; 0.53$ AU

P(R) dR

N
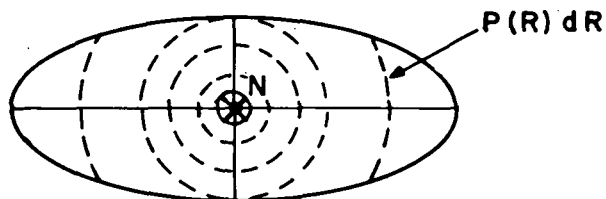
CASE 3 : TARGETING STRATEGY WHEN APPROACHING AT
RIGHT ANGLES TO THE SUN-COMET LINE. $R_{EZ} = 0$
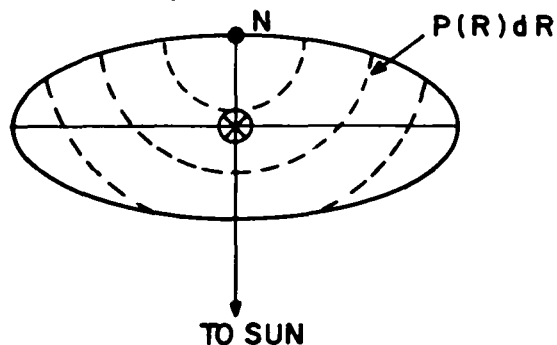$R_\oplus = 0.34$ AU

N

P(R) dR

TO SUN

FIG. 6 - Targeting Strategy

1007
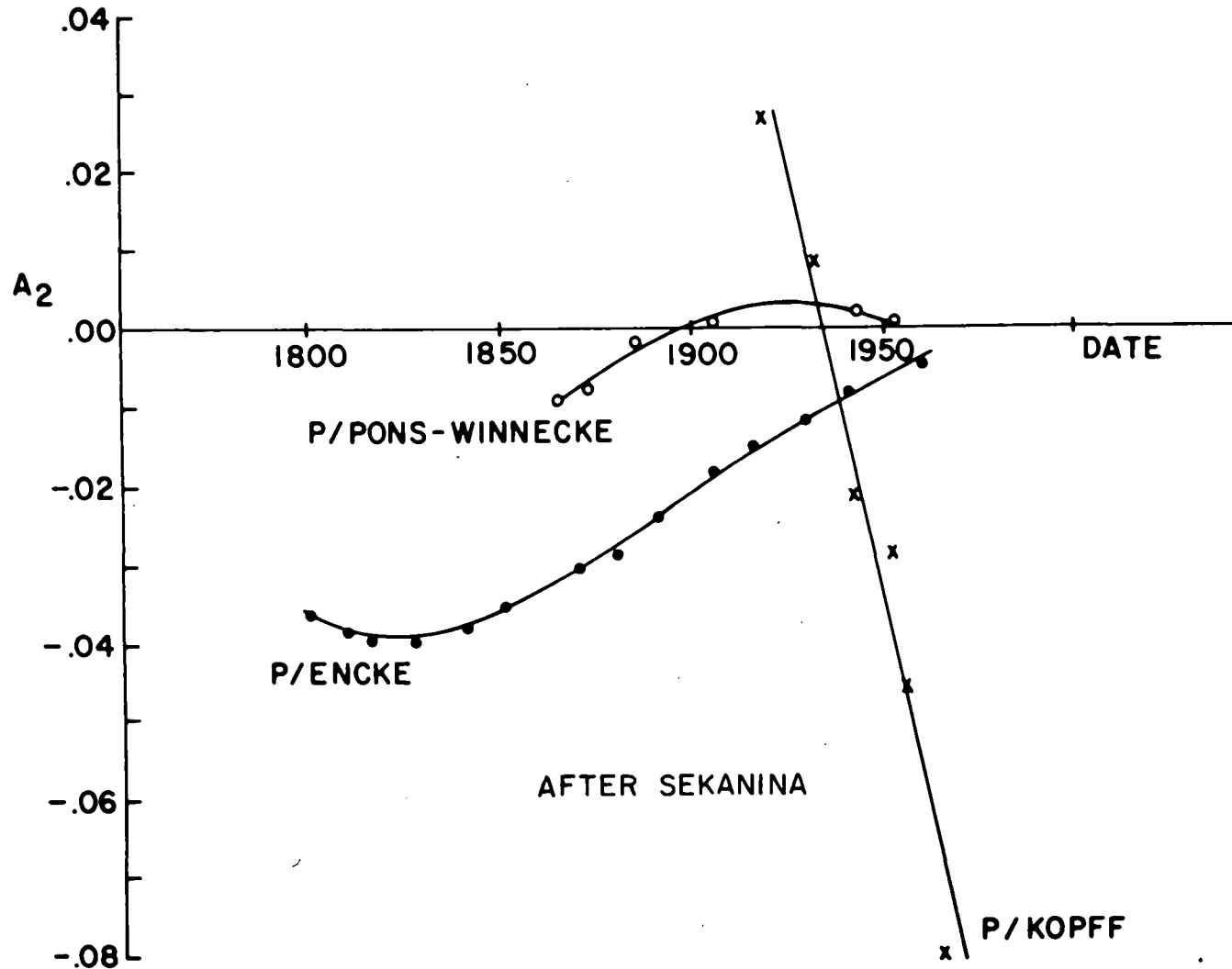
FIG. 7 - Secular Changes in Transverse Nongravitational
Acceleration of Several Short Period Comets

TABLE II: MEDIAN MISS DISTANCE VS. INTERCEPT CONDITIONS

R(A.U.)	ON-BOARD NAVIGATION	MEDIAN MISS DISTANCE (Km) $R_{EZ}^{*}=0$	$R_{EZ}=400$ KM	
0.34	Yes	95 ⎫	471 ⎫	
	No	510 ⎭ Case A**	865 ⎫	
0.53	Yes	98 ⎫	566 ⎬ Case C	
	No	403 ⎬ Case B	1017	
0.80	Yes	62 ⎫	515	
	No	302 ⎭	996 ⎭	

* Radius (Km) of possible Exclusion Zone.

** Targeting strategy, see Fig. 4.

These miss distances are quite realistic and show that the space-craft would definitely pass through the region where ice grains may cause the parent molecule densities to fall below the values predicted by the point source model. Thus, the measured density profiles along the flight path potentially could yield information on any departures from the point source model in this region. Further estimates of the expected science return require establishing a physical model for the comet.

PHYSICAL ACTIVITY MODEL

The combined observations of Beyer[8] and Bortle[9] show that P/Encke has shown some apparent secular decrease in intensity over the past three decades but that it regularly brightens in the same way as it approaches perihelion (Fig. 8). Encke's visual brightness is composed primarily of gas emission (C_2, C_3, CN) and the scattered solar continuum is very weak.[10] Thus, the total magnitudes measured by Beyer and others are primarily gas emissions and can be expected to approach a limiting brightness law of R^{-2} at sufficiently small R. This is so because the total abundance of a certain gas in the coma is proportional to $Q(1 \text{ AU})R^{-2} \times \tau(1 \text{ AU})R^2 \sim Q(1) \tau(1) \sim$ constant, while the fluorescence intensity is proportional to the local insolation times the number of molecules in the coma, or R^{-2}. Second order effects (Swings effect, Greenstein effect) due to doppler shifts, structure in the solar spectrum, etc. play some role for a specific emission, but should average out when the entire set of visible gas emissions is seen. At larger R, the index will first increase but should again approach 2 as reflection from the

nucleus limits the brightness. The index at intermediate R can be quite large ($\sim$ 8.8 for P/Encke at 1.1 AU, Fig. 8). Inspection of Fig. 8 shows that Encke's brightness is fitted reasonably well by an n = 2 law for $.34 \lesssim R \lesssim 0.80$ AU and so we take as our first model assumption:

$$Q_{GAS} \propto R^{-2} \quad .34 \lesssim R \lesssim .80 \text{ AU.} \tag{1}$$

Bertaux et al.[11] have measured the Lyman-alpha emission rate and derived the H-atom production rate from the observed brightness at R = 0.7 AU. They concluded that if the observed H were all produced by dissociation of H_2O, the total production rate of H_2O would be

$$Q_{H_2O} = 3 \times 10^{27} \text{ molecules/sec at 0.7 AU.} \tag{2}$$

We take (2) as our second model assumption. This value for Q_{H_2O} is $\sim$ 100 times smaller than the rates for comets Bennett or Kohoutek.

Ney has shown (earlier paper, this Proceeding) that the thermal infrared emission from P/Encke is $\sim$100 times smaller than that from Comets Bennett or Kohoutek: therefore, we conclude that the gas/dust production rates are nearly the same for these bright new comets and for Encke, a short-period 'old' comet. The lack of visual continuum for Encke relative to Bennett or Kohoutek suggests a very much lower dust albedo for Encke and/or that icy grains contribute most of the visual continuum for Bennett and Kohoutek but are absent in the case of Encke. Our third model assumption is: Encke's dust grains do not possess ice-mantles and so a point-source model for neutral parent
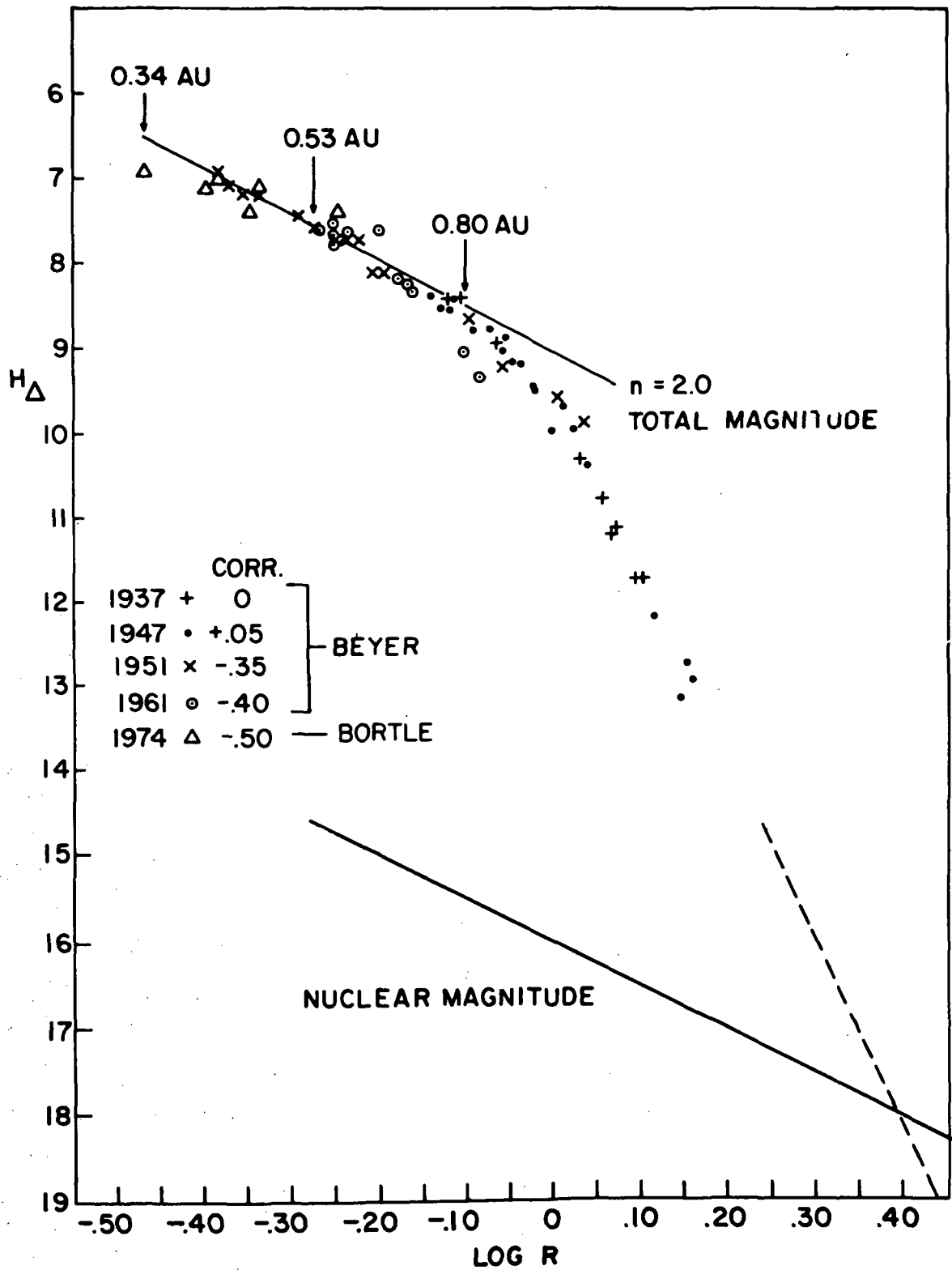
FIG. 8 – P/Encke:Brightness vs Heliocentric Distance

1012

molecular densities is reasonable. As we shall see, the spacecraft neutral mass spectrometer experiment will be capable of verifying the validity of this assumption. For convenience, a uniform radial flow velocity (v_T) of 1 km/second was assumed. This leads to possible underestimates of the densities close to the nucleus where the flow velocity may be smaller, but it is an error on the side of caution.

The H_2O densities in the coma were calculated from the point source model. The total H_2O production rate was normalized to the observed rate at R = 0.7 AU (eqn. 2) and was scaled to other heliocentric distances by R^{-2}, which is valid for the range of R covered by these missions (eqn. 1). A destruction lifetime of τ_1 was taken to be 20 hours, corresponding to a scale length of 7×10^4 km at 1 AU. The simplified flow model is then expressed as:

$$n(D,R) = \frac{n_o(1Km, \ 1AU)}{R^2 D^2} \exp\left(-\frac{(D-1)}{v_T \ \tau_1 R^2}\right), \tag{3}$$

where D is the distance to the nucleus, and

$$n_o(1Km, 1AU) = 1.17 \times 10^{11} \ cm^{-3}. \tag{4}$$

The modelled H_2O densities are shown in Fig. 9. The solid curves include photo-dissociation of the H_2O parent and the dashed portion shows how the densities would fall off in the absence of dissociation.

A lower limit to the radius of P/Encke can be established by assuming that all of the solar radiation incident on the nucleus is effective in vaporizing the H_2O produced at 0.7 AU. This leads to
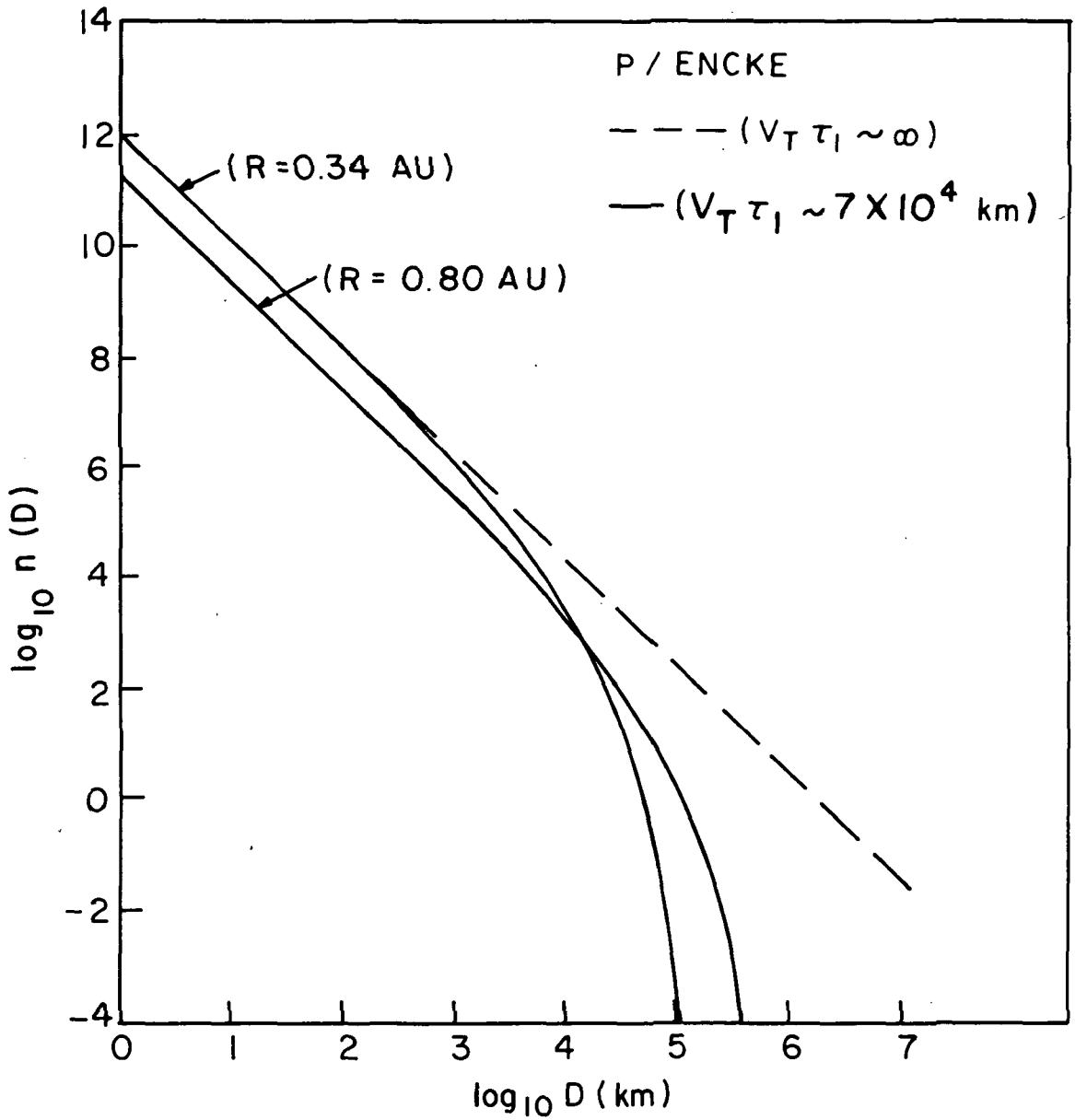
FIG. 9 - H_2O Density vs Distance From The Nucleus

$R > 0.17$ Km. Other estimates can be derived from the observed near-aphelion values of pR^2 which range from 0.7 to 0.2.[12] Extreme estimates for the albedo (0.6-0.03) yield $0.6 \lesssim R \lesssim 4.8$ Km, while nominal albedos of $\sim 0.1 \rightarrow 0.2$ yield $R \sim 2$ Km. For the purpose of assessing the quality of images returned by the imaging experiment we take as our fourth model assumption:

$$R = 1 \text{ Km.} \tag{5}$$

Marsden's recommended nuclear magnitude law[13] was adopted, which implicitly assumes an asteroidal phase law for the nuclear albedo, i.e.

$$N_{mag} = 16.0 + 5 \log\Delta + 5 \log R + .03 \beta, \tag{6}$$

where β is the phase angle (sun-nucleus-observer).[13] The dust distribution was modelled after Finson-Probstein but an upper limit cutoff of ~ 1 cm diameter in the size distribution was introduced based upon the maximum gas flow rates at perihelion.[14] The baseline physical activity model is summarized in Table III.

EXPECTED SCIENCE RESULTS: PARENT MOLECULES

Neutral mass spectrometers of the electron-impact-ionizer class can be divided into two types depending on whether the molecules to be studied are allowed to impact on surfaces in the ionizer region. In the so-called 'fly-through mass spectrometer' the gas streams through the ionizing region and on into the analyzing region without experiencing wall collisions which (at the relatively high impact velocities $\gtrsim 8$ Km/sec) could dissociate and modify the neutral parent molecules. In the so-called 'stagnation

TABLE III

BASELINE PHYSICAL MODEL FOR P/ENCKE

- $R_N > 0.17$ KM; $R_{NOM} = 1$ KM

- $N_{MAG} = 16.0 + 5$ LOG $\Delta + 5$ LOG R $+ .03\beta$

- $T_{MAG} = 8.9 + 5$ LOG $\Delta + 5$ LOG R, IN 1937

  $T_{MAG} \geq 10.3 + 5$ LOG $\Delta + 5$ LOG R, IN 1980 $\bigg\}$ $.34 \leq R \leq .80$

- $Q_{H_2O} \leq 3 \times 10^{27}$ SEC^{-1} AT 0.7 AU

- COLLISIONLESS FLOW MODEL ASSUMED FOR GAS DENSITIES

- DUST DISTRIBUTION MODELED ON FINSON-PROBSTEIN RESULTS FOR

  P/AREND-ROLAND

mass spectrometer', the neutral gases ram into a chamber, collide with walls (becoming thermalized in the process), and eventually effuse out of an orifice. The density in the chamber is higher than the external density by the ratio $V_{SC}/V_{thermal}$ or by $\sim 20 \rightarrow 65$ for the missions considered here and the instrumental sensitivity is enhanced accordingly. However some of the parent molecules are likely to dissociate on impacting the wall surfaces since their kinetic energies exceed their bond dissociation limits. Furthermore, it is impossible to separate the ion signals due to parent molecules from those due to outgassing of the spacecraft materials or from dissociated fragments resulting from wall collisions. The fly-through mass spectrometer does not experience these problems but it has lower sensitivity. The state-of-the-art sensitivity (E) for a Nier-type instrument is $\gtrsim 1$ ion count/sec per 1000 neutral parent molecules/cm^3 (A.O. Nier, private communication). The instantaneous counting rate (dN/dt) on a particular mass peak would be

$$\frac{dN_i}{dt} = E\, n_i \tag{7}$$

where n_i is the local number density for the ith parent molecular species. If the fraction of time spent on the ith mass peak is $G(\%)$, the duty cycle, and the spacecraft velocity relative to the comet is V_{SC}, then the counting rate per unit kilometer of flight path is:

$$\frac{dN}{dl} = \frac{dN}{dt}\frac{dt}{dl} = \frac{GEn_i}{V_{sc}}. \tag{8}$$

The fly-by geometry during close approach is shown in Fig. 10. The integrated number of ion counts in going from L_1 to L_2 can be written (combining eqn. 8 and eqn. 3)

$$\frac{dN}{dl} = \frac{GEQ(R)\exp[-(L^2+D_m^2)^{1/2}/v_T\tau_1 R^2]}{4\pi(L^2+D_m^2)\ V_{SC}\ V_T} = C1(L^2+D_m^2)^{-1}\exp[-C2(L^2+D_m^2)^{1/2}] \qquad (9)$$

or

$$N_{\bar{L},R} = C1\int_{L_1}^{L_2} \frac{Q(R)\exp[-C2(L^2+D_m^2)^{1/2}]}{(L^2+D_m^2)}\ dL \qquad (10)$$

$$N_{\bar{L},R} = F(D,\ R,\ D_m,\ \tau_1,\ Q_1).$$

This calculation was carried out for the various combinations of physical data shown in Table IV, resulting in a total of 48 possible cases. The initial value of L_1 for each case was 32,000 Km. The integration was performed until the error in the number of ion counts ($N^{1/2}$) equalled $\Delta D/\bar{D}$. An 'x' was plotted in the center of the first interval, and the procedure was begun again at L_2. The first measurement to fall below 10% statistical error ($\sqrt{2}\ N^{1/2}$) is marked with a vertical line, and the error of the measurement at closest approach is given (Fig. 11). The curves shown in Fig. 11 are for intercepts at R = 0.34 AU, 0.53 AU, and 0.80 AU reading from top to bottom. These curves show what can be reasonably expected for measurements of H_2O assuming no exclusion zone, improvement of targeting using on-board navigation, a duty cycle of 100% and a lifetime for H_2O of 20 hours at 1 AU. The absence of on-board navigation and introduction of an exclusion zone would increase the miss
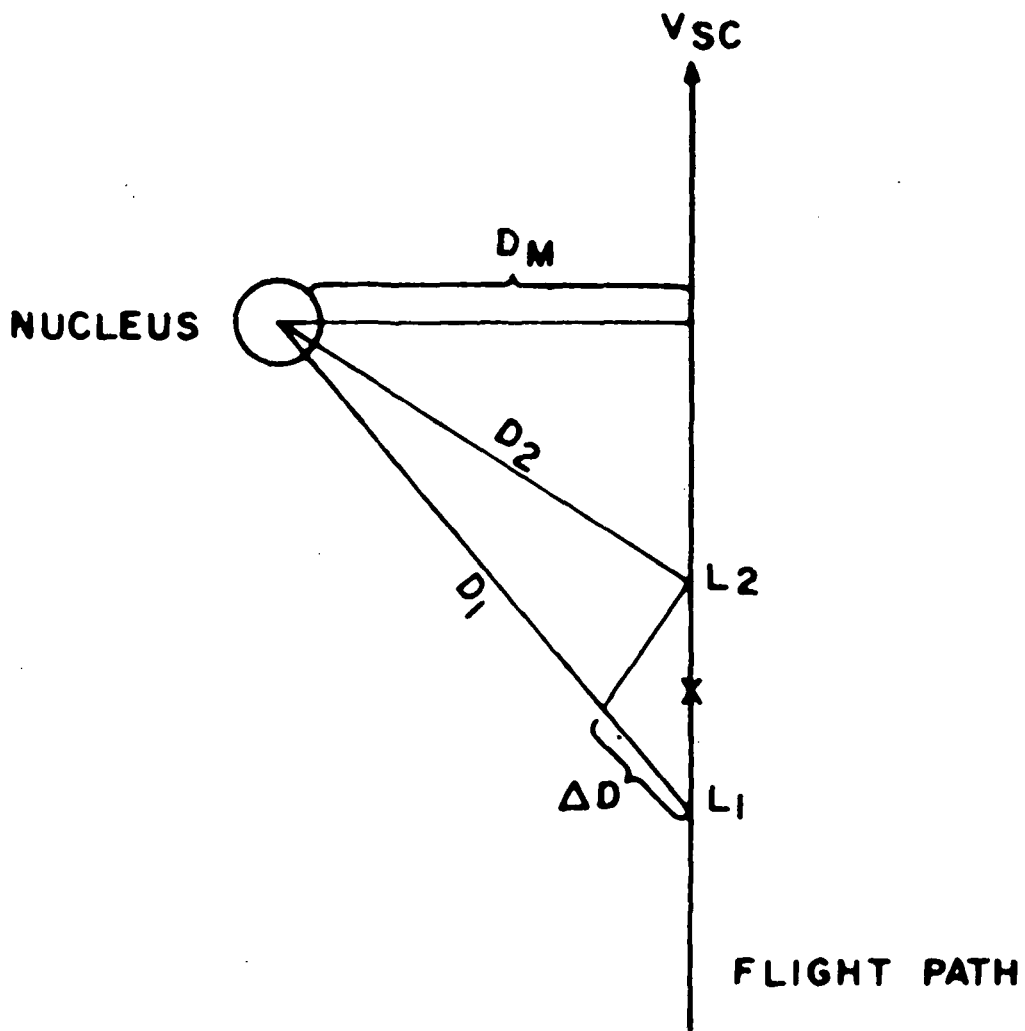
Fig. 10 - Flyby Geometry at Encounter
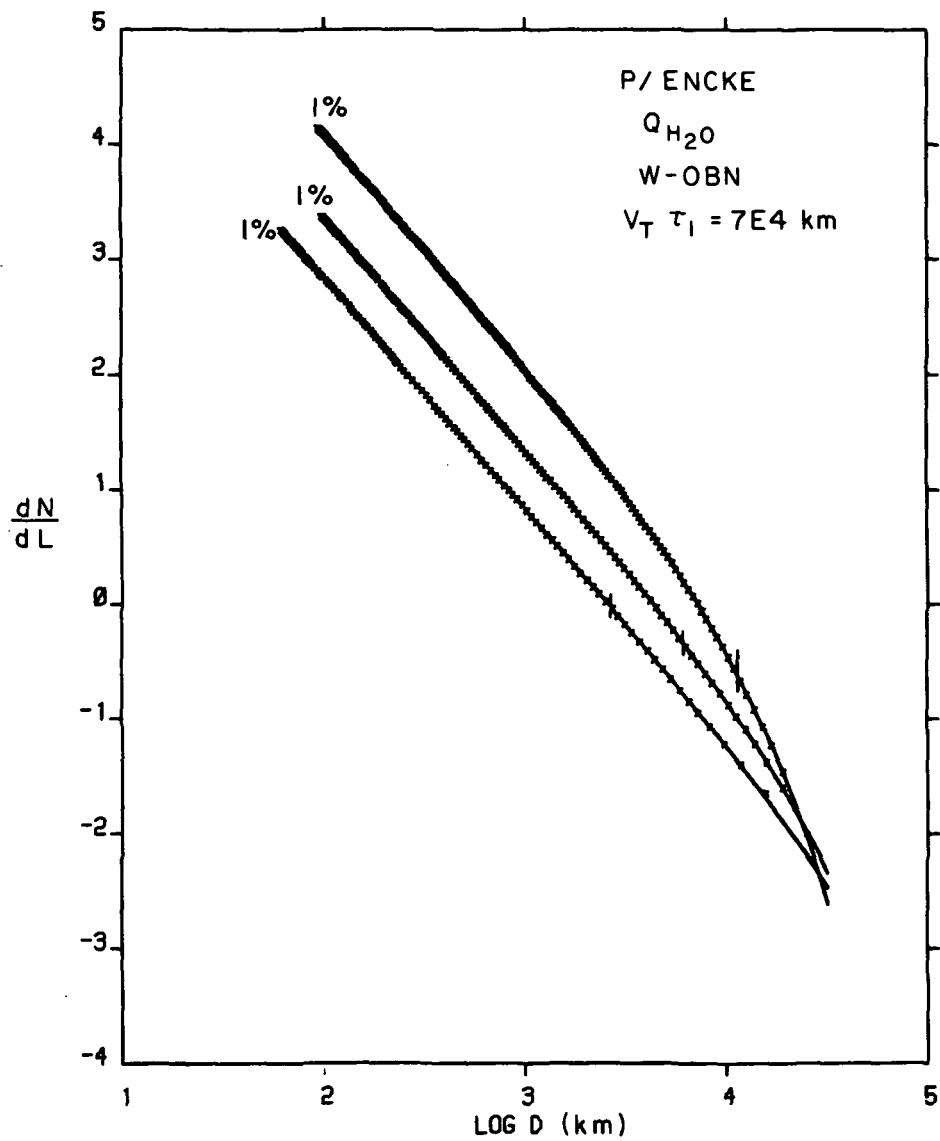
FIG. 11 - Neutral Mass Spectrometer
Results: H_2O

TABLE IV

BASELINE DATA FOR NEUTRAL MASS SPECTROMETER EXPERIMENT MODELS

	MISSION 1 0.34 AU	MISSION 2 0.53 AU	MISSION 3 0.80 AU
C1: Q_{H_2O}	1.26E8	2.31E7	7.0E6
1% Q_{H_2O}	1.26E6	2.31E5	7.0E4
C_2: τ_1 = 7E4 sec	1.23E-4	5.08E-5	2.23E-5
τ_1 = 3.5E3 sec	2.46E-3	1.01E-3	4.44E-4
D_m(Km): R_{EZ} = 0, with OBN	95	98	62
R_{EZ} = 0, without OBN	510	403	302
R_{EZ} = 400 Km, with OBN	471	566	515
R_{EZ} = 400 Km, without OBN	865	1017	996

distances to ~ 1000 Km. If the densities were to fall well below the point source model within 1000 Km of the nucleus, i.e. within a hypothetical icy halo, the existence of same could be verified in the former cases. On the perihelion encounter, the curvature of the density profiles at large distances would also be measureable and the lifetime (scale-length) of H_2O could be determined.

The expected measurements of H_2O at 1% duty cycle (or of a trace molecule with 1% abundance relative to H_2O and a 100% duty cycle measurement) are shown in Fig. 12. This "best case" assumes that on-board navigation is available and that there is no exclusion zone. The flyby distances are then ~ 100 Km but only the perihelion intercept gives reasonable assurance of measuring the trace molecules before entering a hyopthetical icy halo.

From this study, we conclude that the density profiles of H_2O can be measured with high precision over a significant range of distances within the coma on all three missions, but that only the perihelion encounter will enable a determination of the lifetime of the H_2O molecule. Measurements of trace molecules with 1% abundance relative to H_2O will be possible only on the perihelion encounter. These results are based on best estimates of real instrumental sensitivities, well modelled flyby distances, and a reasonable physical activity model for Comet Encke. They show that the neutral mass spectrometer science return is best at perihelion, as intuitively expected.

EXPECTED SCIENCE RESULTS: IMAGING EXPERIMENT

A detailed study of the quality of television images of the nucleus has been carried out by T. Thorpe (JPL) for the Encke Panel. The baseline
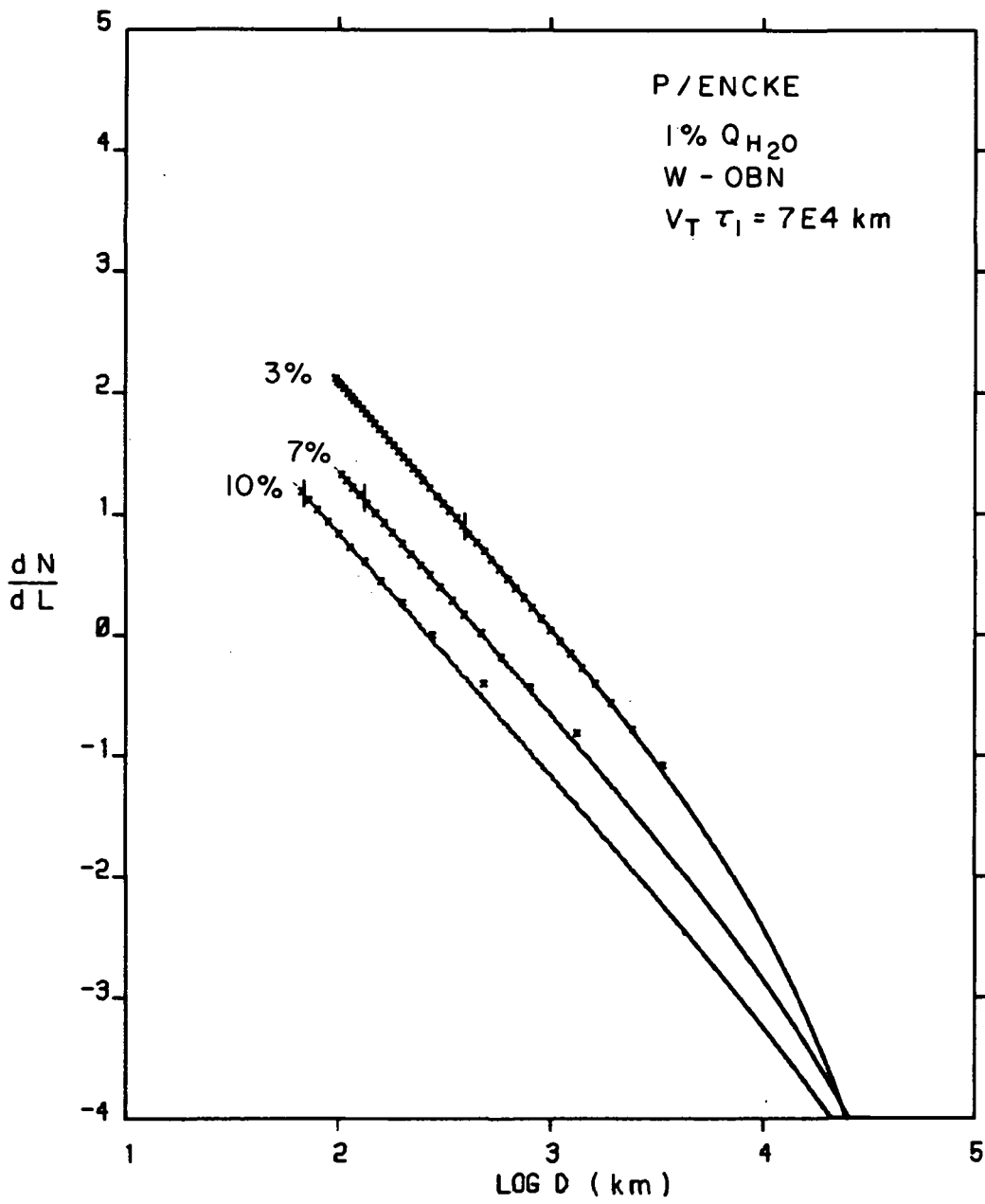
FIG. 12 - Neutral Mass Spectrometer
Results: Trace Molecules

model already discussed was used together with the sensitivity data
for the Mariner 10 vidicon camera to estimate exposure times, smear
rates, linear dimensions of one picture element (pixel) for various
frames, number of pictures returned, and the time in days-before-
encounter for the first resolution of the nucleus. The assumed nuclear
brightness law (eqn. 6) affects the apparent nuclear brightness, as seen
by the spacecraft, through the heliocentric distance (as R^{-2}), through
the nucleus-spacecraft distance (Δ), and through the phase angle (β).
The phase angle is nearly equal to ninety degrees for the intercepts at
0.8 AU and 0.53 AU but can be chosen to be nearly zero degrees for the
perihelion encounter (see Fig. 4 and Fig. 6). Thus the apparent nuclear
brightness is nearly 2.7 magnitudes brighter for the perihelion encounter
on the basis of the phase angle alone. The R^{-2} factor makes the magni-
tude at 0.34 AU another 1.86 magnitudes brighter than at 0.8 AU, for an
overall apparent brightness improvement of 4.56 magnitudes, or a factor
of 66. Shorter exposure times may be used on the perihelion encounter,
leading to reduced image smear from spacecraft motion during the ex-
posure. Also, the smear is further reduced at perihelion because the
spacecraft relative velocity is smaller by a factor of three (8.6/26).
Thus image smear introduced by spacecraft motion is reduced by a factor
of nearly 200 on the perihelion encounter compared with the 0.8 AU en-
counter. This also means that for a fixed exposure time, the smear
on the perihelion encounter images would be three times smaller but
the signal-to-noise ratio would be 66 times greater than on the 0.8 AU
encounter. The results of the imaging study are shown in Table V.

1024

TABLE V

EXPECTED RESULTS OF IMAGING EXPERIMENT ON ENCKE'S NUCLEUS

PARAMETER	R(AU)	$R_{EZ} = 0$* OPTICAL NAVIGATION	NO OPTICAL NAVIGATION	$R_{EZ} = 400$* OPTICAL NAVIGATION	NO OPTICAL NAVIGATION
1. Encounter duration (Image $\geq$ 24 pixels): (seconds)	0.34 AU	606 sec	592 sec	593 sec	568 sec
	0.53 AU	289	284	282	266
	0.80 AU	194	193	190	179
2. Number of pictures possible at 20 sec/frame (Image $\geq$ 25 pixels)	0.34	30	29	29	28
	0.53	14	14	14	13
	0.80	10	10	10	9
3. Encounter Image Resolution at $0°$ phase (10% albedo)**	0.34	6 m	29 m	27 m	49 m
4. Encounter Image Resolution at $90°$ phase (10% albedo) **	0.53	79	54	55	66
	0.80	260	240	230	153
5. Angular Encounter Rate (deg./sec)	0.34	$5°$/sec	$0.9°$/sec	$1.0°$/sec	$0.6°$/sec
	0.53	10.2	2.5	1.8	1.0
	0.80	23.9	4.9	2.9	1.5
6. Linear Image Size at encounter (2 Km nucleus)	0.34	700 pixels	131 pixels	141 pixels	77 pixels
	0.53	680	166	118	66
	0.80	1080	221	130	67

* See Table II for the corresponding flyby distances.

** Midscale Exposure, see ref 1(a), Appendix IV.

Slew rates of 5-10°/sec are mechanically difficult to implement, whereas rates of 1°/sec can probably be achieved. Thus the best image resolution for 0.34 AU is $\sim$ 27 m resolution; for 0.53 AU it is $\sim$ 66 m resolution; and for 0.8 AU it is $\gtrsim$ 153 m resolution. The number of pictures attained is greatest during the perihelion encounter, the signal-to-noise ratio on those frames will be much greater, and the spatial resolution is best on the perihelion encounter.

CONCLUSION

A simple physical activity model has been derived from published data on Encke's comet and has been combined with data provided by realistic mission analyses, and with actual instrumental performance figures to arrive at a quantitative appraisal of the expected scientific results returned by the two most mission-sensitive experiments on a ballistic flyby mission. The expected results have been determined for three specific ballistic intercepts, occurring at heliocentric distances of 0.34 AU, 0.53 AU, and 0.80 AU, respectively. The conclusions confirm the intuitive informed guess: the optimum intercept should occur as near to the perihelion as possible. This is so not only because the comet activity is greatest there, but also because the spacecraft velocity is lowest there. A perihelion intercept would definitely enable measurements of H_2O beginning at $\sim$ 20,000 Km from the nucleus and extending in to $\sim$ 100 Km from it at high accuracy. Trace molecules with 1% abundance relative to H_2O could be measured from $\sim$ 1000 Km in to $\sim$ 100 Km if a 100% duty cycle mass spectrometer with state-of-the-art sensitivity were used. The distances for 'first detections' could be increased by $\sim$ 3 if the ionization efficiency were improved ten-fold.

Approximately 60 or more photographs of the nucleus could be taken with high signal-to-noise ratio on the perihelion encounter, and the resolution of the best frame would be $\sim$ 27 meters. A 2 kilometer diameter nucleus would thus be photographed with $\sim$ 74 resolution elements ($\sim$ 141 pixels) across its diameter, and if circular would show $\sim$ 4300 resolution elements across its disk (at 0° phase angle). This represents the first quantitative assessment of the scientific results which could be obtained on a cometary mission and shows conclusively that such a mission is capable of answering many of the fundamental questions of cometary research.

REFERENCES

1. More detailed information can be found in the following reports:

    a) "Ballistic Intercept Missions to Comet Encke", Final Report
       of the Comet Encke Ballistic Missions Engineering Panel,
       NASA TMX-72542 (1975);

    b) "Cometary Probe to Encke, 1980", Report on the Mission De-
       finition Study, ESRO MS(74)35 (1974);

    c) "Mission Design for a Ballistic Slow Flyby of Comet Encke,
       1980", R.W. Farquhar, D.K. McCarthy, D.P. Muhonen, and
       D.K. Yeomans, NASA TN D-7726 (1974);

    d) "Study of 1980 Comet Encke - Asteroid Missions Using a Spin-
       Stabilized Spacecraft", W.J. Bursnall, E.G. Howard, W.R.
       McMininy, R.G. Shaffer, and J.M. Van Pelt, NASA-CR-114670
       (Summary) and NASA-CR-114671 (Technical Report) (1973);

    e) "Study of Ballistic Mode Comet Encke Mission Opportunities",
       G.R. Hollenback and J.M. van Pelt, NASA CR-137524 (1974);

    f) "Science Aspects of a 1980 Flyby of Comet Encke with a Pioneer
       Spacecraft", L.D. Jaffe, C. Elachi, C.E. Giffin, W. Huntress,
       R.L. Newburne, R.H. Parker, F.W. Taylor, and T.E. Thorpe,
       JPL Report 760-96 (1974);

    g) "Imaging on Ballistic Missions to Comet Encke", L.D. Jaffe,
       D. Bender, R.O. Hughes, B.R. Mackiewicz, and T. E. Thorpe,
       JPL Report 760-112 (1974); and

    h) "A Study of the Solar Electric Slow Flyby of Comet Encke in
       1980", K. L. Atkins et al., JPL Report 760-90 (Rev. A) (1974).

2. cf. "Cometary Spectra", P. Swings, Quart J. Roy. Astron. Soc.
    6, 28 (1959).

3. "Cometary Probes", Rh. Lust, Space Science Rev. 10, 217 (1969).

4. "Comets - Scientific Data and Missions", Proceedings of the Tucson
    Comet Conf., ed. G. P. Kuiper and E. Roemer, Pub. by Lunar and
    Planetary Lab., Univ. of Ariz. (1972).

5. "Proceedings of the Cometary Science Working Group - Yerkes
    Observatory (June 1971)", ed. D. L. Roberts, pub. by ITT
    Research Institute (Dec. 1971).

6. The a-priori ephemeris errors have been discussed by D. Yeomans
    in an earlier paper of these proceedings.

7. Orbital elements after D. Yeomans (private communication, 1974).

8. 1937: M. Beyer, "Physische Beobachtungen von Kometen IV", Astron.
    Nachr. 265, 37 (1938).
    1947: M. Beyer, "Physische Beobachtungen von Kometen VII, ibid.
    278, 217 (1950).
    1951: M. Beyer, "Physische Beobachtungen von Kometen IX", ibid.
    282, 145 (1955).
    1961: M. Beyer, "Physische Beobachtungen von Kometen XII, ibid.
    286, 219 (1962).

9. J. E. Bortle, IAUC 2667 (1974); ibid. 2670 (1974).

10. Cf: "Atlas of Representative Cometary Spectra", ed. P. Swings and
    L. Haser; Technical Report, University of Liege Astrophysical
    Institute, Liege, Belgium (1955);
    "Photoelectric Photometry of Comets", W. Liller, Astron. J. 66,
    372 (1961); and D. Malaise, J. Observ. 44, 144 (1961).

11. "Interpretation of Hydrogen Lyman-alpha Observations of Comets Bennett and Encke", J.L. Bertaux, J. E. Blamont and M. Festou, Astron. and Astrophys. <u>25</u>, 415 (1973).

12. cf. E. Roemer and R.E. Lloyd, Astron. J. <u>71</u>, 443 (1966);

    E. Roemer, IAUC 2435;

    R.E. McCroskey and C.W. Shao, IAUC 2446;

    E. Roemer, IAUC 2446; and

    E. Roemer, IAUC 2586.

13. B. G. Marsden, "Periodic Comet Encke", IAUC 2547 (1973).

14. This part of the study was performed by W. C. Wells, R. S. Benson, A. D. Anderson, and G. Gal (Lockheed Missiles and Space Company) and appears as Appendix III to ref. 1(a).

DISCUSSION

Z. Sekanina: To clear up the question as to what is the current production rate of large dust particles from P/Encke, I suggest that more attention be paid in the future to a possibility of detecting an antitail of this comet. Favorable visibility conditions for such an antitail can be predicted.

M. Dubin: A report of dust relating to Comet Encke was made by Alexander, et al., from measurements of "particle" impacts in Mariner 64. They reported a short-period high flux of particle impact signatures during the brief period when the Mariner spacecraft traversed the orbit plane of Comet Encke.

M. Mumma: Ney's infrared results combined with Bertaux's measurement of the H-atom production rate show that Encke's gas-to-dust production ratio is nearly the same as that for bright comets, i.e., the observed infrared dust brightnesses were ~100 times smaller for Encke and the gas production rates were also ~100 times smaller. On the other hand, Liller has shown that the ratio of continuum to gas emission in the visible is at least 5 times smaller for Encke than for bright new comets, i.e., the product of visual grain albedo and total projected grain area is much smaller for Encke than for bright comets. Assuming similar visual albedos implies that the grain temperature would have to be considerably higher for Encke in order to explain the observed infrared flux. Whipple has suggested for many years that Encke's particle size distribution may be relatively depleted of small particles but have abundant large particles. Thus the observations would seem to be consistent with an abundant large particle flux from Encke.

E. Ney: Our observations on Encke showed a thermal emission continuum at 2 microns to ten microns. This continuum certainly shows that Encke has dust, but the brightness was 100 times dimmer than Bradfield & Kohoutek — down by the same ratio as the Lyman α brightness. It should be pointed out that in passing through the average coma of Encke only about 10 particles per square centimeter would be encountered.

M. Mumma: Wells, et al., have studied Encke's dust distribution and have determined the expected impact rate on a spacecraft during each of the three intercept missions proposed for the 1980 apparition. Their conclusions agree roughly with your estimate.

L. Biermann: I thought our previous discussion had suggested small rather than large grain size as the cause of the high temperature of a grain.

DISCUSSION (Continued)

M. Mumma: An alternate explanation is that the visual albedo is much smaller for Encke's grains than for those of a bright new comet. This would explain both the infrared and visible observations without requiring a temperature excess for Encke's grains, in fact the mean temperature of Encke's grains could be lower than Bennett's or Kohoutek's consistent with larger grain sizes. A corollary is that the visual continuum of Bennett and Kohoutek be contributed primarily by icy grains or ice mantled silicate grains (high albedo) whereas Encke's visual continuum be contributed mainly by grains which do not have an ice mantle and thus have lower albedos. The infrared continuum would be contributed by stripped grains in each case.